ISSN 1063-7761, Journal of Experimental and Theoretical Physics, 2014, Vol. 119, No. 4, pp. 745–752. © Pleiades Publishing, Inc., 2014.
Original Russian Text © A.M. Petrzhik, G.A. Ovsyannikov, A.V. Shadrin, Yu.N. Khaidukov, L. Mustafa, 2014, published in Zhurnal Eksperimental'noi i Teoreticheskoi Fiziki, 2014, Vol. 146, No. 4, pp. 844–853.

ELECTRONIC PROPERTIES OF SOLID

Spin Transport in Epitaxial Magnetic Manganite/Ruthenate Heterostructures with an $LaMnO_3$ Layer

A. M. Petrzhik[a]*, G. A. Ovsyannikov[a,b], A. V. Shadrin[a,b], Yu. N. Khaidukov[c], and L. Mustafa[c]

[a] *Kotel'nikov Institute of Radio Engineering and Electronics, Russian Academy of Sciences, Moscow, 125009 Russia*
**e-mail: petrzhik@hitech.cplire.ru*

[b] *Chalmers University of Technology, Department of Microtechnology and Nanoscience, Gothenburg, S-41296 Sweden*

[c] *Max-Plank Institute for Solid State Research, Stuttgart, 70569 Germany*

Received April 8, 2014

Abstract—Epitaxial $La_{0.7}Sr_{0.3}MnO_3/LaMnO_3/SrRuO_3$ (LSMO/LMO/SRO) heterostructures with an LMO layer 0–35 nm thick are grown by laser ablation on an $NdGaO_3$ substrate at a high temperature. X-ray diffraction and transmission electron microscopy demonstrate sharp interfaces and epitaxial growth of the LSMO and SRO layers in the heterostructures at an LMO layer thickness of 0–35 nm. SQUID measurements of the magnetic moment of the heterostructures with an LMO layer and the data obtained with reflectometry of polarized neutrons show that the manganite LMO layer is a ferromagnet at a temperature below 150 K and strongly affects the magnetic moment of the heterostructures at low temperatures. The magnetoresistance of the mesostructure created from the heterostructure using lithography and ion etching decreases with increasing LMO layer thickness and weakly depends on the direction of an applied magnetic field. If the LMP layer is absent, a negative magnetoresistance is detected; it is likely to be caused by a negative magnetization of the SRO layer.

DOI: 10.1134/S1063776114100161

1. INTRODUCTION

The tunnel junctions that consist of two ferromagnetic electrodes separated by an insulator layer are of interest due to the possibility of creating nonequilibrium spin polarization of carriers and to a practical application in energy-independent magnetic memory [1]. A high tunneling magnetoresistance (TMR), which is required for practical application of such structures, appears when a weak applied magnetic field changes the magnetization direction in one or two of the electrodes. Using the Julliere model [2], we can write the magnetoresistance of the tunnel junction made of two ferromagnets that is induced by the transport of spin-polarized carriers in the form [3, 4]

$$G_{sp} = G_{sp}^0[1 + P_1P_2\cos(\beta_1 - \beta_2)]. \quad (1)$$

Here, G_{sp}^0 is the conductivity of polarized spins, P_1 and P_2 are the spin polarizations, and angles β_1 and β_2 determine the magnetization directions in the ferromagnets. In the limiting cases of antiferromagnetic (antiparallel) and ferromagnetic (parallel) magnetization directions, TMR is determined by the carrier polarization in the two ferromagnets,

$$\mathrm{TMR} = \frac{R_{AP} - R_P}{R_P} = \frac{2P_1P_2}{1 - P_1P_2}, \quad (2)$$

where R_{AP} and R_P are the tunnel junction resistances for the antiparallel and parallel ordering, respectively. When the spin polarization directions of the two electrodes are opposite to each other, R_P is higher than R_{AP} and TMR corresponds to a negative magnetization of one of the electrodes.

The authors of [5, 6] experimentally showed that TMR, which corresponds to a negative magnetic polarization of $SrRuO_3$ of about 10%, takes place in tunnel junctions based on epitaxial $SrRuO_3$ films. However, the calculated values exceed the experimental data and are at a level of –60% [5–7]. As a tunneling layer, an $SrTiO_3$ layer was used in [5, 6]. This difference between the observed and the theoretically predicted polarizations of $SrRuO_3$ can be related to the degradation of the properties of the ferromagnet near the boundary with the insulator, which causes the appearance of a "dead" (nonmagnetic) layer at the boundary [8, 9]. The authors of [8] theoretically showed that the replacement of the $SrTiO_3$ layer by an $LaMnO_3$ layer in the magnetic tunneling structures made of oxide materials substantially increased the magnetoresistance due to better crystallographic and magnetic (because of the absence of a dead layer between the layers) matching between the layers. Note that the theoretical calculations assumed that LMO is an antiferromagnetic dielectric.

In this work, we present the results of X-ray diffraction, magnetic, and magnetic-transport measurements of the heterostructures made of epitaxial $La_{0.7}Sr_{0.3}MnO_3$ and $SrRuO_3$ (hereafter, LSMO and SRO, respectively) films separated by a thin undoped

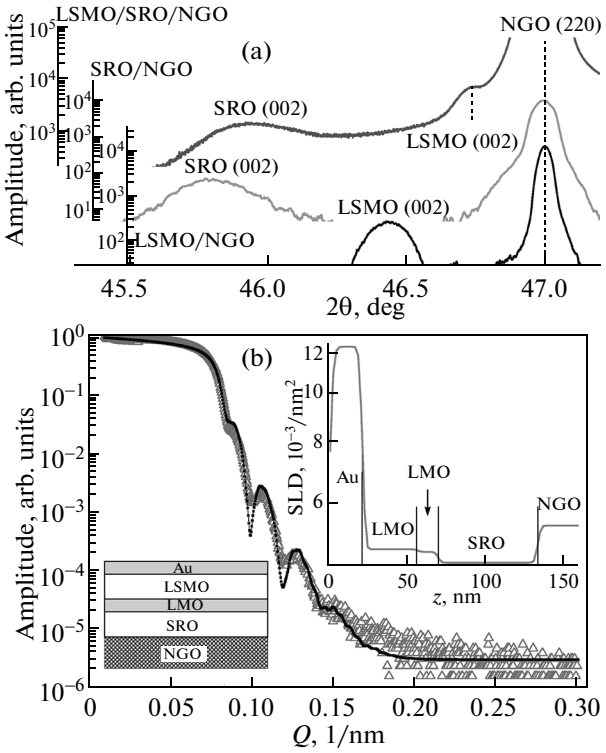

Fig. 1. (a) X-ray diffraction patterns of the LSMO/SRO heterostructure and autonomous SRO and LSMO films grown on an NGO(110) substrate that were recorded in the Bragg reflection geometry. (b) Small-angle X-ray reflection of the LSMO/LMO/SRO heterostructure with a 13-nm-thick LMO layer vs. scattering vector Q. (triangles) Experimental results and (points) calculation for an Au/LSMO/LMO/SRO heterostructure with layer thicknesses 21 nm/36 nm/13 nm/64 nm. The layer thicknesses determined from theoretical approximation agree well with the calibration of the layer growth rate in the laser dependence setup. (inset) Depth profile of SLD vs. the depth of penetration in a sample.

$LaMnO_3$ (LMO) manganite layer. The Curie temperature of an SRO single crystal is $T_{CU} = 163$ K [10, 11] and that of an LSMO single crystal is 364 K [9, 12]. Our earlier works showed that the autonomous epitaxial LMO films grown identically to the heterostructures under study by laser ablation on NGO substrates have a dielectric temperature dependence of conductivity [13]. They have a resistivity more than 100 Ω cm at $T < 100$ K and on the order of 0.1 Ω cm at room temperature. Below $T_{CU} \approx 150$ K, the films are in a ferromagnetic phase, which was measured by ferromagnetic resonance [13, 14].

We used a bilayer Nb/Au film, which ensured a low-resistance contact with LSMO and SRO, as feed electrodes for transport measurements of mesostructures fabricated by lithography and ion etching. At helium temperatures, an Nb film is in a superconducting state and does not contribute to the resistance of the heterostructure, and the contribution of Au may also be neglected due to the use of the four-point probe resistivity measurement method, which excludes the resistance of the feed electrodes. The magnetization of an LSMO film usually lies in the substrate plane, and that of an SRO film is directed at an angle to it [9, 11]. Saturation magnetic fields H_S in LSMO and SRO differ by almost two orders of magnitude [10–12]. In low magnetic fields of about 200 Oe applied in the substrate plane, the LSMO film is expected to undergo magnetization reversal, and these fields are too low for the SRO film to undergo magnetization reversal. The high coercive force of SRO makes it possible to create tunnel junctions without using an additional antiferromagnetic layer to "fix" the direction of the ferromagnetic layer magnetization, which should be constant in an applied magnetic field. The study of LSMO/SRO superlattices using the anomalous Hall effect showed the presence of an antiferromagnetically ordered hole gas at the LSMO/SRO interface [15, 16]. A strong coupling between LSMO and SRO films is also indicated by the shift of the hysteresis loop of the bilayer LSMO/SRO structure induced by an applied magnetic field (exchange bias). The bias direction corresponds to an antiferromagnetic exchange coupling between LSMO and SRO [17]. This effect is absent at temperatures above the Curie temperature of the SRO film.

The purpose of this work is to reveal the effect of an LMO layer 0–35 nm thick on the magnetotransport and magnetic properties of the LSMO/LMO/SRO heterostructure.

2. HETEROSTRUCTURES

Thin LMO, LSMO, and SRO films were grown by laser ablation in the temperature range 700–800°C on a (110) $NdGaO_3$ (NGO) substrate. A heterostructure of total thickness $d_M \sim 100$ nm was grown on a 5×5 mm^2 substrate in a vacuum chamber at a pressure of 0.3 bar. After cooling to room temperature in an oxygen atmosphere, it was coated with a thin (20–30 nm) gold layer. Square mesostructures from 10×10 to 50×50 μm^2 in size were prepared from heterostructures by photolithography and ion-beam etching at low accelerating voltages (100–300 V). Mesostructures of micron sizes were connected to bonding pads of millimeter sizes with an Nb/Au film. Predominant current passage in a mesostructure along the normal to the substrate plane was provided by the insulation of the lateral faces of the mesostructure with an SiO_2 layer.

Epitaxial heterostructure growth was supported by X-ray diffraction and measurements performed on a transmission electron microscope. Figure 1a shows a family of X-ray diffraction patterns for the LSMO/SRO heterostructure, an autonomous SRO film, and an autonomous LSMO film deposited onto an NGO(110) substrate. It is seen in Fig. 1 that the lattice parameter of LSMO in the heterostructure decreases along the normal to the substrate ($a_\perp$), which is caused by the tension of the crystal lattice of

LSMO in the substrate plane ($a_{\parallel}$). Tension $a_{\parallel}$ is likely to be induced by the growth of an LSMO layer on SRO.

The structural properties of the layers and the interfaces were studied by X-ray and neutron reflectometry. The essence of the method consists in measuring the specular reflection coefficient of X-ray or neutron radiation (R_{exp}) when the glancing angle of incident beam θ changes. A modeled curve (R_{mod}) is fitted to an experimental curve (R_{exp}) by minimizing the quantity

$$\chi^2 = \frac{1}{N}\sum_{i=1}^{N}\frac{(R_{exp} - R_{mod})^2}{\delta R_{exp}^2}.$$

where N is the number of experimental points and δR_{exp} is the statistical error of R_{exp}. To calculate a modeled curve, each layer is described using layer thickness d, scattering length density (SLD) ρ, and root-mean-square roughness height σ at the upper interface. The dependence of SLD of a layer containing one type of atoms can be represented in the form $\rho = 4\pi Nb$, where N is the atomic packing density and b is the coherent scattering length. X-ray radiation is scattered by the electron shell of an atom, and the coherent scattering length can be written as $b = r_e Z$, where $r_e = 2.82 \times 10^{-5}$ Å is the classic electron radius and Z is the number of electrons in the atom (i.e., the serial number in the periodic table of elements). In contrast to X rays, the scattering length of neutrons depends on the atomic number of an element in an irregular manner and can differ substantially for different isotopes of the same element. The existence of spin in a neutron makes it sensitive to the magnetic moment of scattering atoms. If the layer has magnetic induction **B** that is collinear to applied magnetic field **H**, the SLD of the layer can be rewritten as $\rho^{\pm} = 4\pi(Nb \pm cB)$, where B is the magnetic induction in the layer and $c = 0.23 \times 10^{-4}$ kG/nm^2. The signs "+" and "–" in this expression mean the projection of neutron spin onto applied magnetic field **H**. If the layer consists of m atoms, the SLD of the layer can be written as

$$\rho = 4\pi N\sum_{i=1}^{m} b_i C_i,$$

where C_i is the concentration of i-type atoms.

To calculate model curves, the exact solutions to a wave equation are used [18]. However, for clarity, we present an expression for the reflection coefficient in the kinematic approximation [18],

$$R_{mod} \approx \frac{1}{Q^4}\left|\sum_{i=1}^{l}(\rho_{j-1} - \rho_j)\exp(iQz_{j-1})\right|^2, \qquad (3)$$

where l is the number of alloys and $Q = (4\pi/\lambda)\sin\theta$ is the angular momentum of a neutron transferred during reflection. Thus, it follows from Eq. (3) that the curves of specular reflection of X-ray and neutron radiation from a multilayer system are the sum of signals from various interfaces with various amplitudes depending on the SLD contrast at them. The joint use of X-ray and neutron reflectometry makes it possible to obtain complete information on the layer thickness, the atomic packing density in each layer, and the interface roughness. In addition, using polarized neutrons, we can obtain information on the depth profile of the magnetization of the structure. To separate a magnetic signal, we can use the spin asymmetry $S(Q) = [R^+(Q) - R^-(Q)]/[R^+(Q) + R^-(Q)]$, where R^+ and R^- are the reflection coefficients of neutrons with spins along and opposite to a magnetic field. Using Eq. (3), we can show that the spin asymmetry depends linearly on the magnetic contrast in the system.

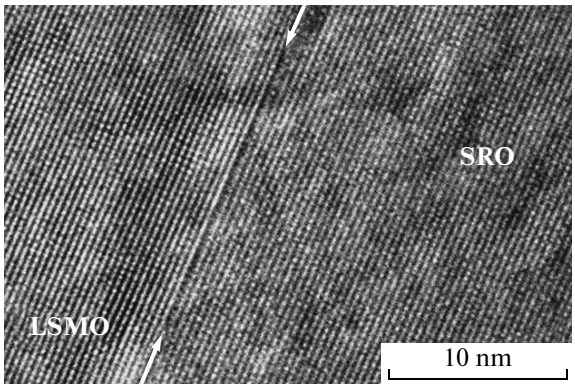

Fig. 2. TEM image of the $SrRuO_3$ (SRO)/$La_{0.7}Sr_{0.3}MnO_3$ (LSMO) interface (JEM-2100 microscope, magnification 800 000). The interface is indicated by arrows.

Figure 1b shows the experimental and calculated X-ray reflectograms measured on a Bruker D8 diffractometer. The depth profile of SLD plotted as a result of fitting is shown in the inset to Fig. 1. It is seen from this profile that the air/gold and gold/LSMO interfaces generate the maximum X-ray radiation contrast; that is, the X-ray reflectogram is most sensitive to the gold layer. The result of fitting gives a gold layer thickness of 21 nm and a gold surface roughness of 2 nm. Note that the layer thickness agrees with the calibration of the laser ablation setup used for layer deposition. Since the sensitivity of X-ray reflectometry to the oxide layer thickness is low, the oxide layer thicknesses were determined by fitting neutron reflectograms (see below).

A thin plate was cut from the initial heterostructure grown on a $5 \times 5 \times 0.5$ mm^3 substrate by focused ion etching and was then studied by transmission electron microscopy (TEM). Figure 2 shows the image of the cross section of the SRO/LSMO heterostructure taken with a Jeol JEM-2100 transmission electron microscope. Detailed TEM analysis of the interface with corrected aberration in SRO/LSMO heterostructures showed that Mn and Ru atoms are mixed on the scale of one atomic cell and Sr and La atoms are mixed on the scale of two atomic cells [15]. Electron-energy-loss spectroscopy demonstrated that this interface is

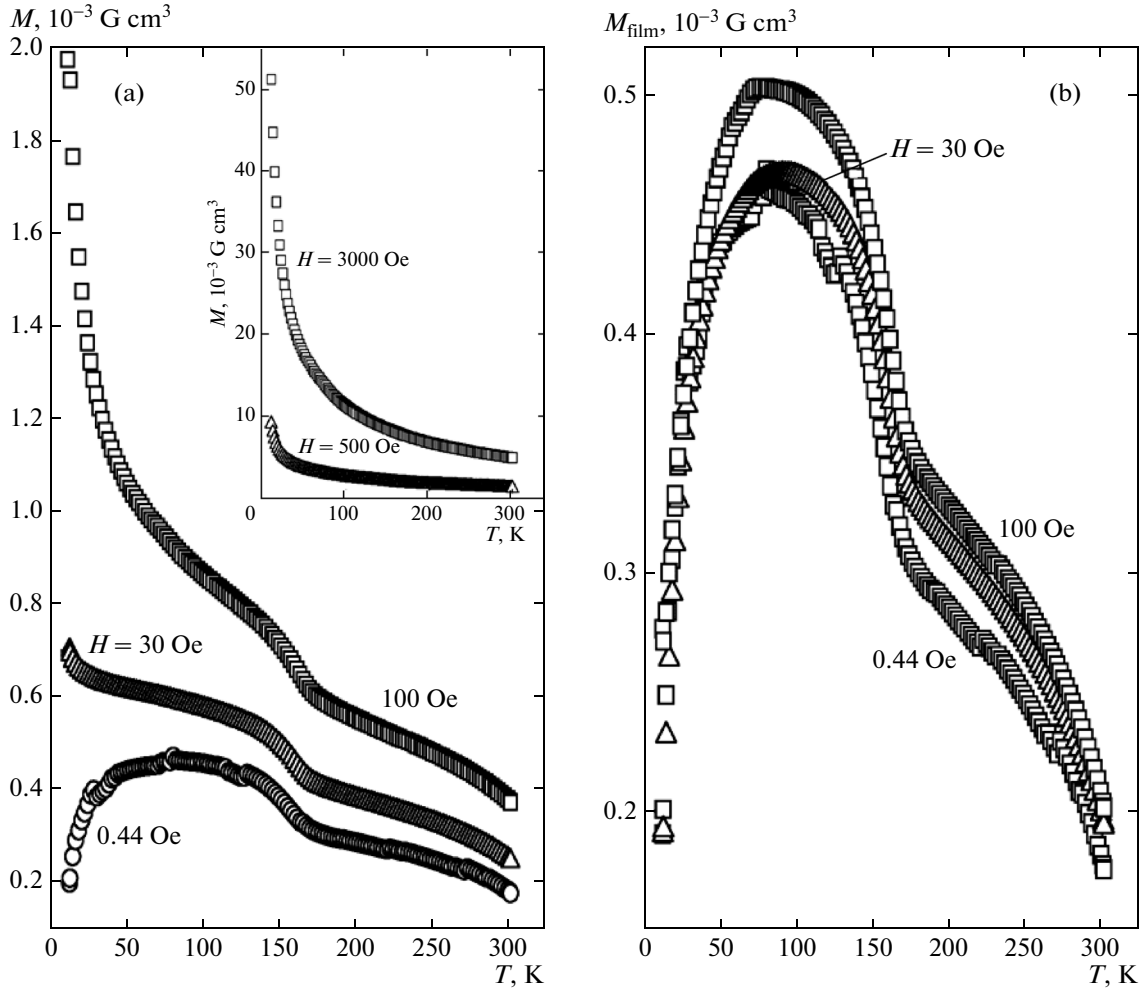

Fig. 3. (a) Magnetic moment in the substrate plane vs. temperature for an epitaxial LSMO/LMO/SRO heterostructure grown on an NGO(110) substrate at $d_{LMO} = 13$ nm. (b) The magnetic moment of the LSMO/LMO/SRO heterostructure minus the paramagnetic component of the NGO substrate.

also characterized by a nonuniform oxygen vacancy distribution on a scale of 1–2 nm [15, 20].

The magnetic properties of the heterostructures were studied by SQUID magnetometry and polarized neutron reflectometry (PNR) [18] in the temperature range 4–300 K when a magnetic field is applied in the substrate plane. Figure 3 shows the temperature dependences of the heterostructure magnetization measured in heating a sample after preliminary magnetic field cooling. As is seen from Fig. 3a, the paramagnetic NGO substrate significantly contributes to the magnetic moment of the heterostructure. This effect becomes most pronounced at low temperatures, which hinders the estimation of the magnetization of thin films. To subtract the substrate contribution, we used the temperature curve measured at $H = 3000$ Oe. Figure 3b shows the results of calculation provided that the contribution of the NGO substrate contribution at $H = 3000$ Oe is well above the contribution of the epitaxial films. This condition is grounded by the $M(H)$ dependence, which has the shape of a hysteresis loop with a saturation field of 400 Oe at $T = 10$ K. Above $H = 400$ Oe, a linear change in $M(H)$ is observed, which is related to the contribution of the NGO substrate. As is seen in Fig. 3b, the magnetic moment increases with decreasing temperature in the temperature range 170 K $< T <$ 300 K, which is characteristic of the magnetization of the LSMO layer below the Curie temperature. Then, the magnetic moment increases at temperatures below 170 K. According to [13, 14], this behavior is likely to be caused by the transition of the LMO layer into a ferromagnetic state. Apparently, the contribution of the SRO layer magnetization can increase simultaneously. At temperatures below 100 K, the magnetization decreases. The decrease in the magnetic moment at temperatures below 100 K cannot be unambiguously interpreted. Nevertheless, the authors of [19] reported similar appearance of an antiferromagnetic compo-

nent in bilayer LSMO/SRO heterostructures upon freezing in low magnetic fields.

The data obtained with a SQUID magnetometer were complemented with PNR data. Since PNR is a technique based on the magnetic contrast of an interface, it has no problems with a paramagnetic signal from a substrate, in contrast to SQUID magnetometry. The measurements were carried out on the NREX polarized neutron reflectometer at the FRM II (Munich, Germany) research reactor using a sample with a layer thickness $d_{LMO} = 13$ nm in the temperature range $T = 4$–300 K and a magnetic field $H = 30$ Oe after the sample was frozen in a magnetic field $H = 4$ kOe. Figure 4a shows the R^+ and R^- curves of specular reflection of polarized neutrons measured at $T = 200$ K, which is higher than the Curie temperature of the SRO layer and much lower than the Curie temperature of the LSMO layer. When analyzing the curves of specular reflection of polarized neutrons, we were able to restore the scattering length profiles of neutrons polarized along and opposite to the field (inset to Fig. 4a; dashed and solid lines, respectively). As follows from the SLD curves, the presence of a magnetic field in the LSMO and LMO layers makes it possible to distinguish them. The layer thicknesses obtained from the fitting of the neutron reflectometry curves for a heterostructure with an LMO layer of thickness $d_{LMO} = 13$ nm (according to the calibration of the sputtering setup) were $d_{LSMO} = 37.4 \pm 0.3$ nm, $d_{LMO} = 19.1 \pm 0.3$ nm, and $d_{SRO} = 44.9 \pm 3$ nm. According to fitting, the magnetization in the LSMO layer at $T = 200$ K is $4\pi M_{LSMO} = 5.00 \pm 0.03$ kG, which corresponds to $2.7\mu_B$ per manganese atom. Note that the values of SLD of the oxide layers and the magnetic moment of manganese atoms agree with the data in [17, 21]. When the temperature decreases below 150 K, the spin asymmetry oscillation amplitude increases strongly near $Q = 0.2$ nm^{-1} (Fig. 4b). A quantitative calculation shows that the spin asymmetry at $T = 140$ K can be described by the introduction of an additional magnetization $4\pi M_{LSMO} = 4.2$ kG ($2.4\mu_B$/Mn) in the LMO layer. The related increase in the magnetic moment agrees with the SQUID magnetometry data presented in Fig. 3b.

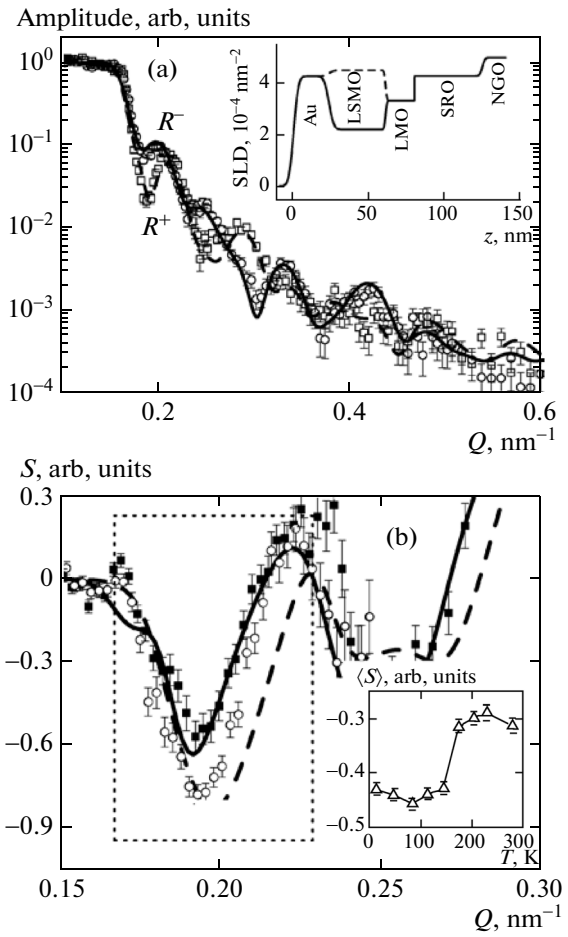

Fig. 4. (a) (points) Experimental and (solid curves) calculated curves of specular reflection of polarized neutrons for a heterostructure with a 13-nm-thick LMO layer that were measured at $H = 30$ Oe and $T = 200$ K. (inset) The depth profile of SLD for neutrons polarized (dashed curve) along and (solid line) opposite to a field. (b) (points) Experimental and (curves) calculated spin asymmetry of scattering measured at a temperature of (dashed curve) 200 and (solid line) 140 K. (inset) Temperature dependence of the average spin asymmetry in the range 0.17–0.23 nm^{-1}.

3. MESOSTRUCTURES

The inset to Fig. 5 schematically shows the mesostructure made from the heterostructure. An electric current passes through the SRO film and the LMO/SRO, LMO/LSMO, and Au/LSMO interfaces. Figure 5 shows the resistance of mesostructure R_nA ($A = L^2$ and R_n is the mesostructure resistance at a voltage of 1.5 mV and $T = 4$ K) as a function of mesostructure linear size L. The value of R_nA should not change in the case of a uniform current passage in a mesostructure with interfaces. In our case, R_nA increases with the linear size, which indicates a nonuniform current passage in the mesostructure. Additional measurements of the Au/SRO and Au/LSMO [14, 22] interfaces showed that the Au/LSMO interface mainly contributes to the resistance. Taking into account the fact that the electrical resistivities of the SRO and Au films are well below that of LSMO, we can estimate the current spreading length in the mesostructure using the formula [23, 24]

$$L_S = \frac{R_nAd_{LSMO}}{\rho_{LSMO}}. \quad (4)$$

Substituting the values $R_nA = 1.5 \times 10^{-5}$ Ω cm^2 and $\rho_{LSMO} = 10^{-4}$ Ω cm, we obtain $L_S \approx 8$ μm at an LSMO film thickness $d_{LSMO} = 40$ nm for the mesostructures with an LMO layer. For the mesostructures without an LMO layer, L_S increases slightly because of an increase of R_nA. Therefore, a nonuniform current distribution

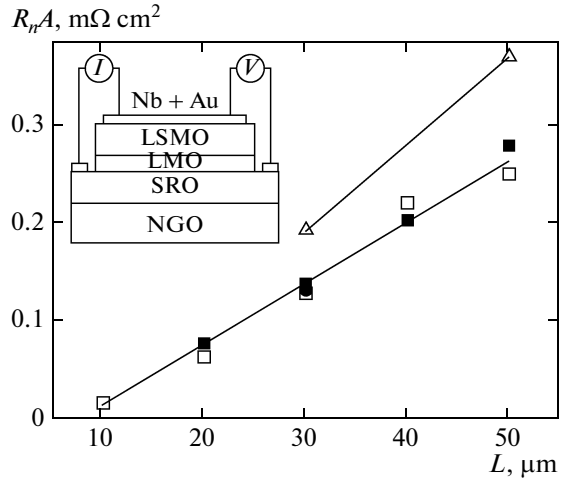

Fig. 5. Product of resistance R_n into mesostructure area A vs. linear mesostructure size L at $T = 4$ K. The solid lines illustrate linear approximation. d_{LMO} = (△) 0, (□) 4.7, and (■) 3.5 nm. The cross section of the mesostructure is schematically shown in the inset.

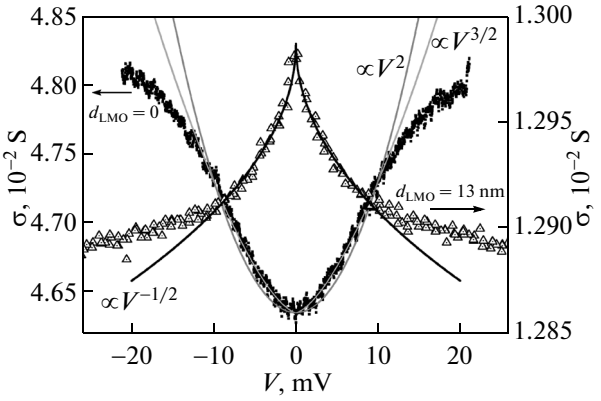

Fig. 6. Differential conductivity vs. the bias voltage for mesostructures with d_{LMO} = (points) 0 and (triangles) 13 nm.

in the substrate plane is observed in most measured mesostructures.

Figure 6 shows the conductivity of mesostructures with $d_{LMO} = 0$ and 13 nm versus the applied voltage. The decrease in conductivity σ at low voltages V points to a tunneling character of the current passage through the mesostructure without an LMO layer [25]. Indeed, the averaged (over the quasiparticle momentum direction) interface transparencies estimated from R_nA by the formula [24, 26, 27]

$$\overline{D} = \frac{2\pi^2\hbar^3}{e^2p_F^2}\frac{1}{R_NA} = \frac{2\rho^{LSMO}l^{LSMO}}{3R_NA}, \quad (5)$$

turn out to be rather low, $D = 10^{-5}$–10^{-4}. Here, p_F is the minimum Fermi momentum from LSMO and Au at the following parameters: $\rho^{LSMO}l^{LSMO} \approx 10^{-10}\ \Omega\ \text{cm}^2$ and $R_nA = 1.5 \times 10^{-5}\ \Omega\ \text{cm}^2$. The authors of [28–30] considered the carrier scattering by magnetic excitations, which causes a nonlinear field dependence. The model of scattering of spin-polarized carriers [30] implies the following dependence for conductivity of a magnetic contact:

$$\sigma(V) = \sigma_0 + \sigma_2|V^2| + \sigma_{3/2}|V^{3/2}|, \quad (6)$$

where the term $\sigma_2|V^2|$ is determined by bulk magnons and $\sigma_{3/2}|V^{3/2}|$ is determined by surface antiferromagnetic magnons. As is seen in Fig. 5, both terms of the $\sigma(V)$ dependence satisfactorily describe the experimental data at voltages lower than 10 mV. At higher voltages, $\sigma(V)$ strongly deviates from dependence (6).

The structures with $d_{LMO} \geq 10$ nm demonstrate a radically different voltage dependence of conductivity $\sigma(V)$, which cannot be described by a tunnel junction with two metallic ferromagnetic electrodes. In this case, the model of two ferromagnets separated by a normal metal can be most appropriate [31]. At low voltages $V < 10$ mV, the $\sigma(V)$ dependence is well described by the relation $\sigma(V) \propto V^{-1/2}$.

4. MAGNETORESISTANCE OF THE MESOSTRUCTURES

Figure 7a shows a family of magnetic-field dependences of mesostructure resistance $R(H)$ normalized by resistance R_0 measured in the absence of a magnetic field ($H = 0$). The LMO layer thickness changes from zero to 13 nm. It is seen that mesostructure resistance $MR^* = (R_0 - R)/R_0$ decreases with increasing magnetic field or the LMO layer thickness (also see the inset to Fig. 7a). At $d_{LMO} = 0$, MR* has the maximum value and the $R(H)$ dependence has a weak hysteresis; that is, $R(H)$ depends on the direction of a change in the magnetic field (Fig. 7b). At $d_{LMO} = 0$, the magnetoresistance for the antiparallel location of magnetizations (R_{AP}) is much lower than the resistance during ferromagnetic ordering (R_P); therefore, following Eq. (2), we can assume the presence of a negative magnetic polarization in one of the mesostructure layers. The absolute polarization of the SRO film determined from Eq. (2) is $P = -0.35\%$ on the assumption of 100% polarization of the LSMO film at low temperatures. This value is well below the polarization of SRO detected in structures with an $SrTiO_3$ layer [5, 6]. A nonuniform current distribution in the mesostructure is likely to weaken the effect of the negative magnetic polarization of SRO on the $R(H)$ dependence. At $d_{LMO} > 10$ nm, no negative magnetic polarization of SRO is observed in the experimental $R(H)$ dependence.

The authors of [8] theoretically showed that the use of an LMO layer in magnetic tunneling structures substantially increases the magnetoresistance due to better crystallographic matching and the absence of a dead (nonmagnetic) layer at the interface between structure layers. The main assumption in the theoreti-

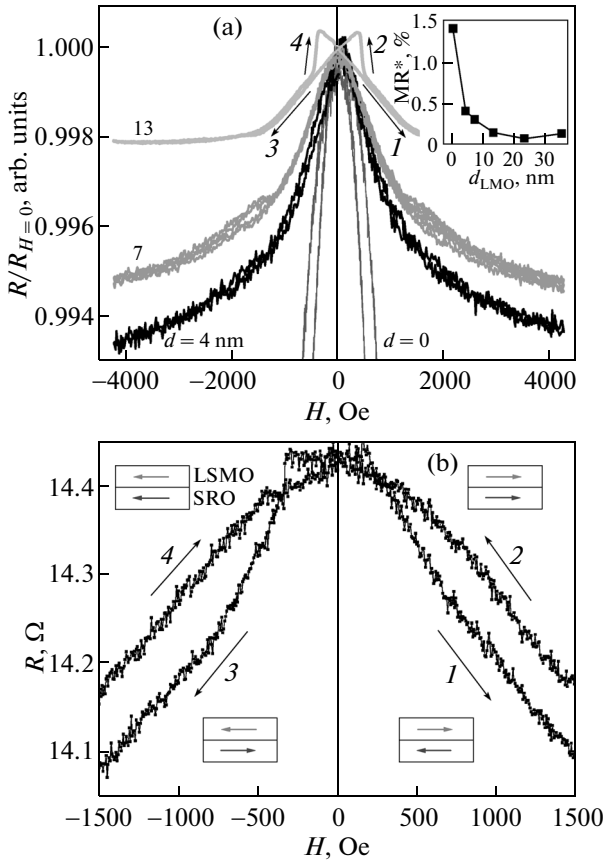

Fig. 7. (a) Family of dependences of the magnetoresistance of a mesostructure on the magnetic field at $d_{LMO} = 0$, 4, 7, and 13 nm and T = 4.2 K. (inset) MR* = $(R_{H=0} - R_{H=0.1\,T})/R_{H=0}$ as a function of d_{LMO}. (b) Magnetoresistance of the mesostructure without an LMO layer ($d_{LMO} = 0$). The sequence of a change in the applied magnetic field is indicated by arrows. (insets) Orientation of the magnetizations of two mesostructure electrodes in the substrate plane.

cal calculations was the fact that LMO was an antiferromagnetic insulator. However, ferromagnetism with a Curie temperature of about 150 K appears in real epitaxial LMO films [13, 21]. As a result, all three layers in the LSMO/LMO/SRO structure turn out to be ferromagnetic. We assume that it is ferromagnetism in the LMO layer in our case that decreases MR* with increasing d_{LMO}. At d_{LMO} = 13 nm, we observed a hysteresis in the $R(H)$ dependence at low magnetic fields.

5. CONCLUSIONS

Using a SQUID magnetometer and the reflectometry of polarized neutrons, we studied the magnetic properties of $La_{0.7}Sr_{0.3}MnO_3/LaMnO_3/SrRuO_3$ (LSMO/LMO/SRO) heterostructures. At an $LaMnO_3$ layer thickness of 6.5 and 13 nm, we detected a sharp increase in the magnetic moment in the substrate plane at temperatures $T \le 170$ K, which is related to an increase in the magnetization of the SRO and LMO layers. The magnetization of the LMO layer below T = 150 K reaches $4\pi M_{LMO}$ = 4.2 kG ($2.4\mu_B$/Mn).

At temperatures $T \le 100$ K, a SQUID magnetometer detected a decrease in the magnetic moment in the substrate plane. This decrease can be related to the exchange interaction observed in SRO/LSMO structures; it results in antiferromagnetic ordering at the interface. In our case, LSMO and SRO layers are separated by an LMO layer, which is most likely to be an insulator and limits the interaction between LSMO and SRO. Therefore, we can exactly state about the causes of the observed behavior of magnetization only after performing an additional neutron experiment upon zero-field cooling. The magnetoresistance of the LSMO/LMO/SRO mesostructure decreases with increasing LMO layer thickness. However, a magnetic field hysteresis exists in fields of several hundred oersteds at a layer thickness d_{LMO} = 13 nm. In the absence of an LMO layer, the $R(H)$ dependence exhibits a magnetoresistance induced by a negative magnetization of the SRO film. This magnetoresistance is likely to be substantially determined by an oxygen-nonstoichiometric LMO layer, which becomes ferromagnetic and conducting, and by nonuniform current spreading in the prepared mesostructures of micron sizes.

ACKNOWLEDGMENTS

The authors are grateful to I.V. Borisenko, V.V. Demidov, Yu.V. Kislinskii, K.I. Konstantinyan, A.E. Sheierman, T. Keller, and B. Kaimer for assistance in performing the experiments and fruitful discussions. Special thanks are due to A.A. Klimov and S.A. Nikitov for helpful discussions.

This was supported by the Russian Foundation for Basic Research (project nos. 14-07-00258, 14-07-93105), a grant from the President of Russia for support of leading scientific schools (project no. NSh-4871.2014.2). This study was performed using the unique scientific nanotechnology equipment of the Center for Joint Use of the Moscow Institute of Physics and Technology. The neutron measurements were carried out on the NREX instrument at the Heinz Maier-Leibnitz Zentrum, Garching, Germany. G.A. Ovsyannikov acknowledges the support of European foundation FP 7 in terms of the program Research Infrastructures (project no. 283883).

REFERENCES

1. I. Zutic, J. Fabian, and S. D. Sarma, Rev. Mod. Phys. **76**, 323 (2006).
2. M. Julliere, Phys. Lett. A **54**, 225 (1975).
3. J. C. Slonczewski, Phys. Rev. B: Condens. Matter **39**, 6995 (1989).
4. R. Gunnarsson, Z. G. Ivanov, C. Dobourdieu, and H. Russel, Phys. Rev. B: Condens. Matter **69**, 054413 (2004).

5. D. C. Worledge and T. H. Geballe, Phys. Rev. Lett. **85**, 5182 (2000).
6. K. S. Takahashi, A. Sawa, Y. Ishii, H. Akoh, M. Kawasaki, and Y. Tokura, Phys. Rev. B: Condens. Matter **67**, 094413 (2003).
7. J. Singh, J. Appl. Phys. **79**, 4818 (1996).
8. S. Yunoki, E. Dagotto, S. Costamagna, and J. A. Riera, Phys. Rev. B: Condens. Matter **78**, 024405 (2008).
9. V. V. Demidov, G. A. Ovsyannikov, A. M. Petrzhik, I. V. Borisenko, A. V. Shadrin, and R. Gunnarsson, J. Appl. Phys. **113**, 163909 (2013).
10. A. Kanbayasi, J. Phys. Soc. Jpn. **41**, 1876 (1976).
11. G. Koster, L. Klein, W. Siemons, G. Rijnders, J. S. Dodge, C.-B. Eom, D. H. A. Blank, and M. R. Beasley, Rev. Mod. Phys. **84**, 253 (2012).
12. Y. Moritomo, A. Asamitsu, and Y. Tokura, Phys. Rev. B: Condens. Matter **51,** 16491 (1995).
13. I. V. Borisenko, M. A. Karpov, and G. A. Ovsyannikov, Tech. Phys. Lett. **39** (12), 1027 (2013).
14. A. M. Petrzhik, G. A. Ovsyannikov, A. V. Shadrin, K. I. Konstantinyan, A. V. Zaitsev, V. V. Demidov, and Yu. V. Kislinskii, J. Exp. Theor. Phys. **112** (6), 1042 (2011).
15. A. Y. Borisevich, A. R. Lupini, J. He, E. A. Eliseev, A. N. Morozovska, G. S. Svechnikov, P. Yu, Y.-H. Chu, R. Ramesh, S. T. Pantelides, S. V. Kalinin, and S. J. Pennycook, Phys. Rev. B: Condens. Matter **86**, 140102(R) (2012).
16. M. Ziese, F. Bern, A. Setzer, E. Pippel, D. Hesse, and I. Vrejoiu, Eur. Phys. J. B **86**, 42 (2013).
17. X. Ke, L. J. Belenky, C. B. Eom, and M. S. Rzchowski, J. Appl. Phys. **97**, 10K115 (2005).
18. J. Daillant and A. Gibaud, *X-Ray and Neutron Reflectivity Principles and Applications* (Springer-Verlag, Berlin, 1999), ISSN 0940-7677.
19. X. Ke, L. J. Belenky, V. Lauter, H. Ambaye, C. W. Bark, C. B. Eom, and M. S. Rzchowski, Phys. Rev. Lett. **110**, 237201 (2013).
20. M. Ziese, I. Vrejoiu, E. Pippel, P. Esquinazi, D. Hesse, C. Etz, J. Henk, A. Ernst, I. V. Maznichenko, W. Hergert, and I. Mertig, Phys. Rev. Lett. **104**, 167203 (2010).
21. J.-H. Kim, I. Vrejoiu, Y. Khaydukov, T. Keller, J. Stahn, A. Rühm, D. K. Satapathy, V. Hinkov, and B. Keimer, Phys. Rev. B: Condens. Matter **86**, 180402(R) (2012).
22. G. A. Ovsyannikov, A. E. Sheierman, A. V. Shadrin, Yu. V. Kislinskii, K. I. Konstantinyan, and A. Kalabukhov, JETP Lett. **97** (3), 145 (2013).
23. A. M. Klushin, A. Golubov, W. Prusseit, and H. Kolstedt, J. Low. Temp. Phys. **106**, 265 (1997).
24. F. V. Komissinskii, G. A. Ovsyannikov, N. A. Tulina, and V. V. Ryazanov, J. Exp. Theor. Phys. **89** (6), 1160 (1999).
25. W. F. Brinkman, R. C. Dynes, and J. M. Rowell, J. Appl. Phys. **41**, 1915 (1970).
26. F. V. Komissinskii, G. A. Ovsyannikov, and Z. G. Ivanov, Phys. Solid State **43** (5), 801 (2001).
27. A. V. Zaitsev, Sov. Phys. JETP **59** (5), 1015 (1984).
28. M. Paranjape, J. Mitra, A. K. Raychaudhuri, N. K. Todd, N. D. Mathur, and M. G. Blamire, Phys. Rev. B: Condens. Matter **68**, 144409-1 (2003).
29. A. M. Petrzhik, G. A. Ovsyannikov, V. V. Demidov, A. V. Shadrin, and I. V. Borisenko, Phys. Solid State **55** (4), 759 (2013).
30. F. Guinea, Phys. Rev. B: Condens. Matter **58**, 9212 (1998).
31. Yu. G. Naidyuk, O. P. Balkashin, V. V. Fisun, I. K. Yanson, A. Kadigrobov, R. I. Shekhter, M. Jonson, V. Neu, M. Seifert, S. Andersson, and V. Korenivski, New J. Phys. **14**, 093021 (2012).

Translated by K. Shakhlevich